Observation, prediction, and modeling atmospheric structure effects on EO/IR systems

Michael J. Kendra
Atmospheric and Environmental Research, Inc.
Delia Donatelli
Air Force Research Laboratory/VSBYB
James H. Brown
Air Force Research Laboratory/VSBYB
James M. Griffin
Atmospheric and Environmental Research, Inc.
Hilary E. Snell
Atmospheric and Environmental Research, Inc.

Atmospheric structure may be extracted from measured scenes and used in conjunction with conventional radiative transfer codes to model stressing atmospheric radiance conditions. We describe techniques that allow us to efficiently insert the extracted scene enhancements into ambient scenes created using models such as MODTRAN, SHARC, and SAMM2. We present examples of structured radiance enhancements, such as aurora, polar mesospheric clouds (PMC), and stratospheric warmings, which have been recombined with ambient model background scenes. The structure features are added to ambient model scenes such that they are properly located in the global/geophysical environment, accounting for the dependence of specific types of atmospheric structure on time, latitude, and season, in order to ensure real world fidelity.

We recognize that there are several limitations to this approach, and use existing model capabilities to overcome these limitations. In the case of aurora, we show how auroral observations in the infrared by the MSX SPIRIT III radiometer can be used to determine valid model inputs. In the case of stratospheric warmings, we use measured scenes to determine stratospheric temperature enhancements. We demonstrate that proper combination of validated model inputs allows simulation of complex scenes in a real world context, and that prediction can be extended to other IR bands.

1. INTRODUCTION

Infrared (IR) sensors observing the background environment through the earth's atmosphere are adversely affected by spatial and temporal variations in atmospheric radiance and transmission along the sensor line of sight (LOS). The physics of stochastic fluctuations is largely understood, and the radiation transport theory and models that include stochastic effects exhibit high fidelity when compared to corresponding sensor measurements. Deterministic structure is not as well understood, however, and the associated radiance levels and variability are often significantly higher than those of the benign, stochastic background. Since the radiance measured by the sensor comes from both the object of interest and the radiating atmosphere, and it can also be attenuated by the atmosphere along the optical path, separation of these components is required in order to extract the information content of the object. We list a variety of phenomena responsible atmospheric structure in the earth limb in Table 1.

IR radiance models that account for deterministic structure and clutter are needed to predict the occurrence and impact of atmospheric structure on IR sensing systems. These models need to address real world variability in operational settings, so they should have the ability to assimilate real-time measurements when available. These models must provide realistic predictions for times or regions for which real-time data are not readily available, so they must include climatological model components capable of using either sparse or no data inputs. The ability to use measurements from one wavelength to predict structure and clutter at other wavelengths must be developed. Results must be made available in near real-time, so the real world computational time need for a set of predictions cannot exceed the initial forecast time increment. Predictions must be scalable to other lines of sight and wavelengths, and must be easy to apply and understand in operational settings.

Table 1. Summary of earth limb effects.

Phenomenon	Altitude (km)	Latitude (deg)	Season	Time of Day	Effect on Clutter
Aurora	<150	high	all	night	increase
Terminator	<120	all	all	dawn/dusk	increase
Temperature Inversions	30-90	all	all	all	increase
PMC	60-85	high	summer	day	increase
Airglow Layer	70-100	all	all	all	increase
NRER Variations	>80	all	all	all	increase
Waves	25-95	all	all	all	increase
Stratospheric Warming	30-80	>30	winter	all	increase
SPRITES	40-150	low, mid	all	all	increase
Bores	80	all	all	all	increase

2. LIBRARY OF EXTRACTED SCENES

The process we used to identify, extract, and validate radiometrically-stressing phenomena is illustrated schematically in Fig. 1. As described previously, stressing conditions were identified in the radiometric measurements. These scenes were then examined in more detail to determine the source of the radiance enhancement, such as clouds, aurora, or temperature effects, so they could be classified by phenomenological type and catalogued in the database. From a stressing scene of interest, we developed methodologies to extract phenomenological enhancements from the background radiance. This part of the process is illustrated in Figs. 1a and b, and will be described in detail below. The extraction techniques are somewhat different for different phenomena, so each phenomenon is treated differently.

After an enhancement has been successfully extracted, it can be added directly to an ambient background scene constructed from the radiance codes. This is illustrated in Fig. 1d, where we show the extracted enhancements added to a SHARC model scene. In a sense, the objective is to make the model more sensor-like and the sensor more model-like. If this can be done in a reversible fashion and the processes are joined in the middle, a sensor scene can be made to look like a model scene, or a model scene look like a sensor scene. One advantage of doing this is shown in Fig. 1 where the altitude range of the simulated scene is extended compared to that of the measured scene.

Validation of the extraction process was done by simulating conditions similar to that of the observation using standard scene generation tools such as SHARC or SAMM [1]. The un-modeled phenomena were then added to the simulated scene to create a composite scene of the background atmosphere plus the stressing condition. This scene was then compared qualitatively with MSX data to ensure that the phenomenon had been captured appropriately. This validation process ensures consistency in the overall scene radiance calculation.

There are several difficulties and limitations in adding extracted phenomena back into model scenes. Scene location, line-of-sight, geophysical conditions, and sensor characteristics must be similar, unless it can be demonstrated that these have little effect. Issues related to extensibility for specific phenomena often involve elements of known characteristics and climatology since it is important to locate the structure in a setting where it might be observed. The issue of spectral dependence is also critical, and we placed a high priority on developing and demonstrating techniques that produce realistic results for all spectral bands.

The scene extraction is accomplished in two ways. One is to create a high-fidelity ambient model scene that matches the conditions of a measured scene as closely as possible, and to treat any difference as being due to the identified atmospheric structure. A basic limitation of this approach is that enhancements extracted in this manner are restricted with respect to the sensor bandpass, and possibly to orbital conditions and line-of-sight as well. A second way is to create specific model inputs such that the model scene matches the measured scene as closely as

possible. This approach is difficult to accomplish because it entails knowledge of the physical causes, a sense of how to alter the model inputs to reflect environmental conditions, and numerous model runs to adjust the model inputs such that the desired fidelity is achieved between the modeled and measured scene. However, the approaches are complementary because, when successful, the second approach addresses many of the limitations of the first, since model output accounts for wavelength dependencies and line-of-sight effects. Scene extraction is useful for some aspects of validation and will play a role in determining sensor effects, as described later.
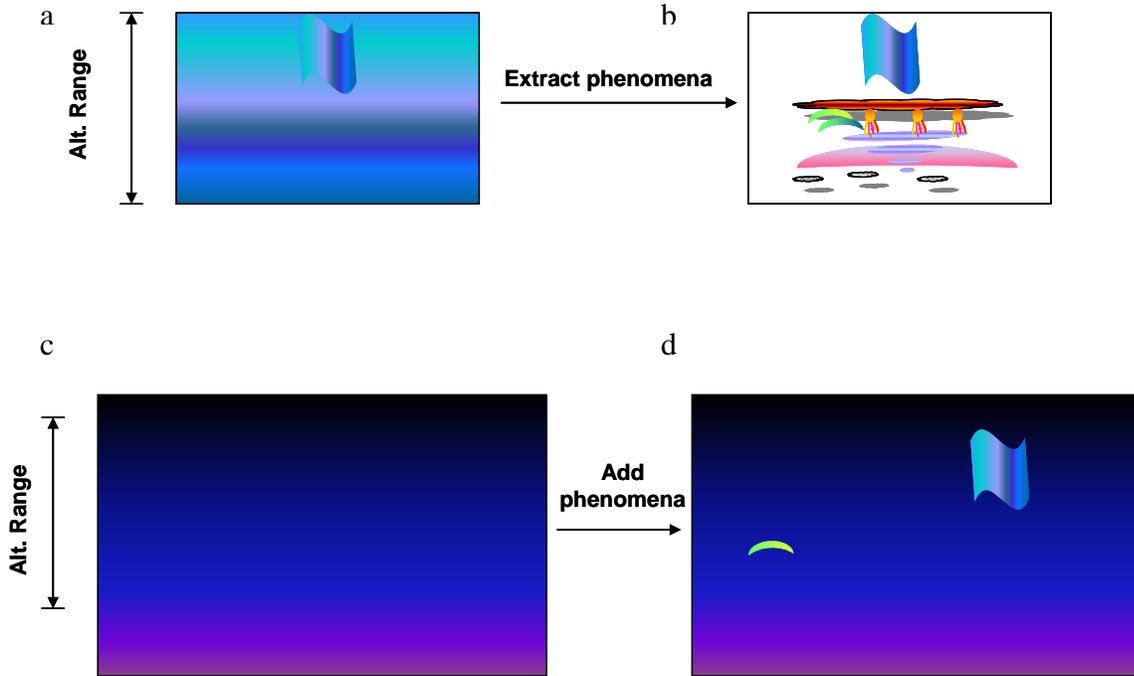

Fig. 1. Conceptual diagram: a) measured scene, b) extracted enhancement, c) SHARC model scene, and d) SHARC model scene plus enhancement.

3. SCENE MODELING AND SIMULATION

3.1 Polar Mesospheric Clouds

Limb-viewing measurements of polar mesospheric clouds (PMCs) were observed on numerous occasions in MSX Bands C and E. In Band C, the PMC radiance was often a factor of 30 or more above ambient levels. We examined MSX experiments specifically designed to measure PMCs under favorable viewing conditions, where the presence of PMCs in the scene could be confirmed by simultaneous observation in the ultraviolet, visible, and infrared.

Climatologies of PMCs have been developed using both ground- and space-based observations at visible wavelengths. While these studies provide valuable insight, it is not clear that they are applicable to infrared observations, and the user of our empirical library must also have information about the correct placement (spatial and temporal) of PMCs. We took the approach of using microphysical models to predict regions of likely PMC formation. The basis for our microphysical model is the temperature dependence of the saturation vapor pressure of water vapor over ice. Saturation ratio (sometimes called supersaturation ratio) is a function of the temperature and vapor pressure of water, $S=p_v/p_{sat}(T)$, where p_v is the partial pressure of water vapor in the atmosphere and $p_{sat}(T)$ is the saturation pressure of water vapor over ice at temperature T. Values of S greater than 1 indicate regions where PMC occurrence is likely, with the probability of PMC observation increasing with increasing S. PMC formation cannot occur if the saturation ratio is less than 1, and if the PMC environment changes such that this ratio drops below 1 the ice particles will sublime. We have added this model to SAG 1 and SAG 2, using the SAG temperature and water vapor number density to compute saturation ratio of water vapor over ice at each altitude and automatically determine the likelihood of PMC conditions.

As shown in Fig. 2, we demonstrated that Polar Mesospheric Cloud (PMC) occurrence could be predicted reliably using a microphysical model of the saturation ratio of water vapor over ice. Figs. 2a-c show model saturation ratios for three corresponding measurements of PMC shown in Figs. 2d-f. We integrated this model into SAG as part of this effort.

We developed a SAG driver program capability to compute ratio values over a geographic grid for any region, date, and time of interest, and a second program to extract the maximum ratio at each grid point. We used this first program to process northern hemisphere at three-hour time steps during May through August 2005. We used the second program to process the SAG output files and generated a time series of PMC saturation ratios. The time series used to extract the maximum saturation ratio of water vapor over ice along with the associated water vapor number density, temperature, and altitude for each geographic point within a fixed spatial grid. As part of the process, the PMC grid generator program ingested the historical geophysical indices (Ap, F10.7 and F10.7bar) from a database built from NOAA online archives. Execution time averaged about 20 minutes to generate a daily set of SAG files (at 3 hour increments). An additional two minutes were needed to read a daily set of SAG files and generate the final hemispheric grid files for that day. A full season of SAG files were generated and processed in approximately 22 minutes*n days.

We used idl to read the maximum saturation ratio data base and produce a set of PNG files containing continental outlines and the PMC-related parameter on interest on a false-color scale. These were imported into PowerPoint and configured to run as a slide show movie. Highlights from these images are shown in Fig. 3, where we show results over polar cap at 0h UT for 4 July 2005 in Fig. 3a and summarize the PMC seasonal changes at 0h UT in Fig. 3b. We note that saturation ratios greater than 1 indicate likely regions of PMC observation.
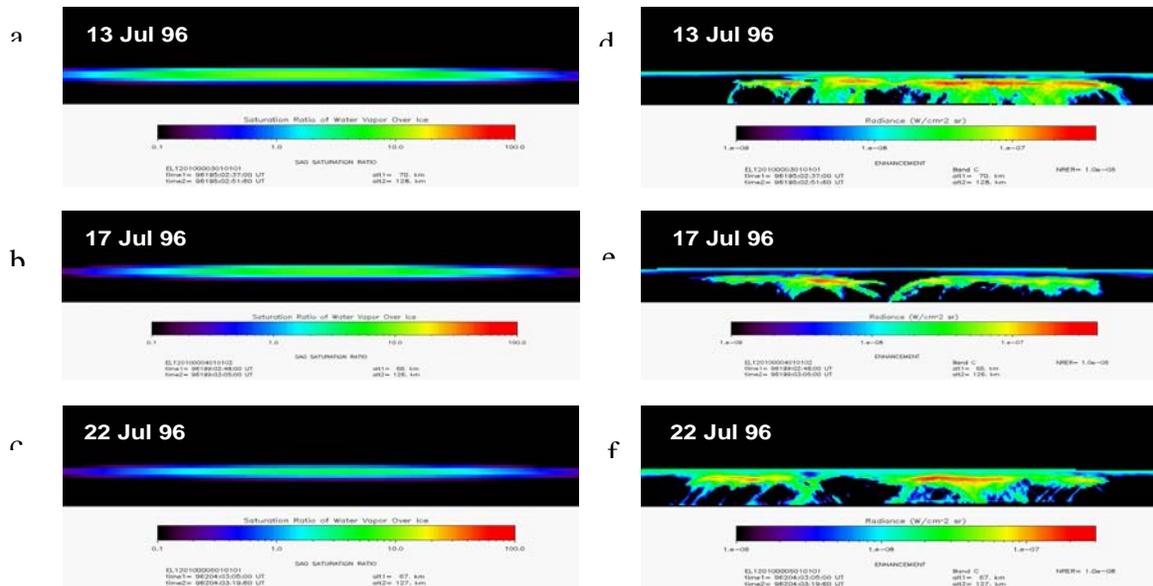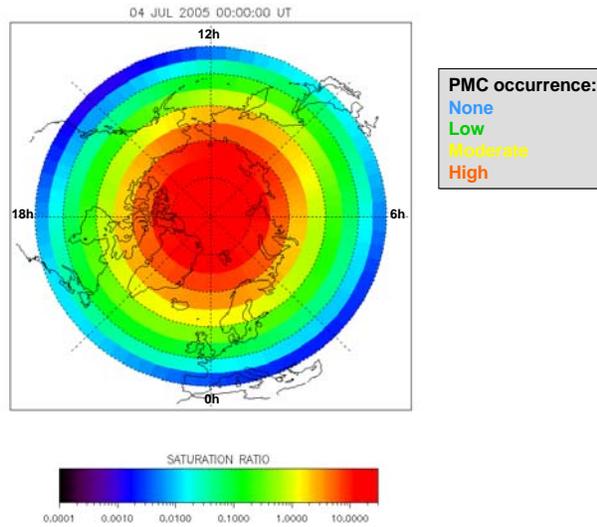

Fig. 2. a-c) Saturation ratio of water vapor over ice during three PMC observations. d-f) Extracted MSX band C PMC enhancements from band C measurements.

There is no program for real-time detection of PMC, although several ground facilities and active satellites detect and report on their occurrence. We believe this PMC observational data is too sparse to be of great value for general application, but it should be useful for validation of this work. The SABER instrument on the TIMED satellite produces temperature profiles at PMC altitude, and we have already developed software to use these data in SAG.
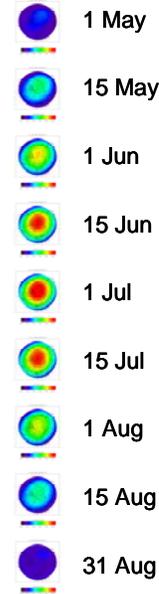
Fig. 3. Forecast saturation ratio of water vapor over ice over the northern polar cap on a) 4 July 2005, and b) 1 May through 31 August 2005. Ratios greater than 1 indicate regions of probable PMC occurrence.

3.2 Stratospheric Warming and Temperature Inversion Thermal Structure

A small number of MSX limb measurements included the stratosphere, and during some of these there was evidence of thermal anomalies in MSX Bands B, C, and E. These measurements were made in the northern hemisphere during winter, and on two occasions we were able to confirm the presence of stratospheric warmings using other sources. Warmings are thought to be caused by disruptions in the global circulation pattern of the atmosphere, and are characterized by elevated temperatures at and below the stratopause. They were typically observed at tangent altitudes from 30-60 km, and the temperature in this region may be elevated by 30 K or more, resulting in enhancements of a factor of 2-3 for all bands. Evidence of waves is also observed in these regions, suggesting atmospheric turbulence.

We were able to model thermal structure by adjusting SAG temperature profiles such that the model and measured radiances agreed over a range of altitudes. Taking the difference between the validated modified temperature profiles and the original ambient model profiles, we produce a set of temperature difference profiles that can then be applied to model temperature profiles for different scenarios. These, in turn, can be used in a series of model runs to simulate scenes, and the effects of temperature-induced enhancements can be simulated for any sensor band under all conditions.

We also utilized data products from the TIMED satellite SABER instrument. We acquired data for one orbit during a reported stratospheric warming event [2] and developed techniques and software to assimilate SABER temperature profiles into SHARC. A FORTRAN-based software package was developed for replacing the standard MSIS model temperature profile in SAG atmosphere files with SABER data product temperatures. To accomplish this, the code reads a SABER level 2A data file to extract the temperature profiles of interest and associated information concerning profile locations and timelines. For each of these profiles, the code runs SAG to generate a nominal atmosphere file. Since the duration of each SABER temperature profile is approximately 17 seconds, the location and time tag associated with the midpoint of the profile is used for the SAG run. The SAG atmosphere is then read into a memory buffer. Linear interpolation is used to map the SABER measured temperature profile to the altitude bins of the MSIS model profile. The buffered data is written to a SAG atmosphere file using a different file name. The code also generates a special input file for use by the SHARC manager program, developed by us to queue and manage SHARC runs.

We show SAG and SABER temperature profiles for 14 February 2002 in Fig. 4a, where the MSIS temperature profile is shown in black and the SABER profile in red. MSIS90 was used to compute SAG 0.92 temperatures. We

note an elevated stratospheric temperature in the SABER data below 56 km compared to SAG. To run SHARC with SABER temperatures, we use linear interpolation of the SABER data to replace SAG temperature at the discrete altitudes required by SHARC. The use of linear interpolation is justified because the resolution of the SABER data is about 0.4 km whereas SAG temperature profile resolution is 2 km in this altitude region. The altitude resolution employed by SHARC/SAG is sometimes insufficient in that it does not allow the full variability of the assimilated data to be taken into account. We show MSX band B simulated scenes created from SHARC model runs using SAG temperature and SABER temperature in Figs. 4b and c respectively. The SABER-based simulation in Fig. 4c shows the effect of the stratospheric warming (red) in the lower portion of the image, and demonstrates the improvement realized by using temperature measurement to drive the SHARC model. In the context of sensor battlespace application, the SAG scene (Fig. 4b) predicts no impairment (green) while the SABER scene (Fig. 4c) predicts severe impairment (red).
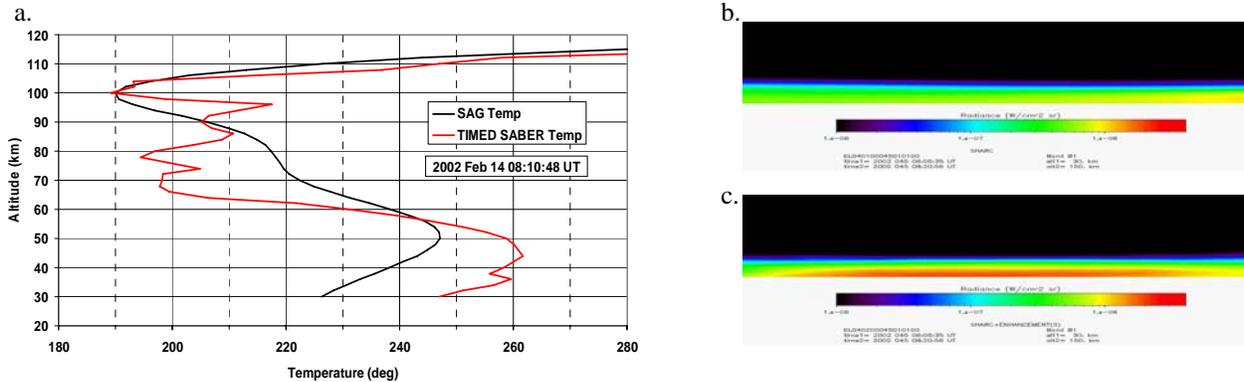

Fig. 4. a) Original SAG model temperature profile (black) and TIMED SABER temperature profile (red). The resolution of the SAG profile is limited to 2-km steps from the cutoff altitude of 30 km and higher. The stratopause (local maximum near 40 km), moved from 52 km for the SAG profile to 45 km for the SABER and increased by approximately 15 Kelvin, indicating a stratospheric warming measured by SABER. b) Simulated MSX band B model scenes for 14 February 2002 using SAG model temperature profiles, and c) TIMED SABER measured temperature profiles.

3.3 Aurora

Auroral signatures were observed on many occasions in MSX Band B limb measurements. While CO_2 fluorescence is a dominant source of daytime emission within Band B, auroral structure is the dominant nighttime source, often a factor of 100 or more above ambient background levels. This auroral emission is from two species, CO_2 and NO^+, and CO_2 self-absorption can affect the scene if the emission region is beyond the tangent point. Selection of a suitable auroral scene was a challenge because we needed a case that could be validated.

3.3.1   SHARC Auroral Inputs from MSX Radiometer Band B Measurements

For auroral inputs, SHARC4 requires the user to define a dosing region, the type of electron energy deposition (dosing) associated with this region, and its dosing history. The dosing region is specified by the geographic sub-points of four corner and the lower and upper altitude limits. The type of dosing is governed by whether it follows a *Maxwellian* or *Gaussian* distribution and by the energy and energy flux characteristics of the distribution. The dosing history is defined by both the *duration* of the dosing and the *time offset* relative to the start of the dosing when the modeled observation is made. Maxwellian distributions typically characterize continuous aurora features, whereas the Gaussian distributions usually characterize discrete aurora arcs. Because the MSX auroral scenes we selected were spatially diffuse, subsequent discussion is limited to Maxwellian distributions.

One way to specify the dosing in SHARC is to select from three pre-defined International Brightness Coefficient (IBC) auroral classes. These classes are represented by Maxwellian distributions that are defined by two parameters: the total electron flux energy in erg cm^{-2} sec^{-1}, and the characteristic energy in KeV. Table 2 summarizes the model parameters for these IBC classes.

A significant number of MSX Earthlimb events were designed to make measurements in the auroral region, so aurora were observed in band B on many occasions. We use a database of quality-assured MSX SPIRIT III radiometer measurements [3] for all MSX related comparisons. These events served as the basis for our work with the SHARC auroral model inputs. In preparation for defining and validating a set of auroral parameter inputs to SHARC, a representative test case was needed to ensure that a reasonable comparison could be made between the band-integrated profile of the SHARC model results and an equivalent profile from a measured scene. The selected scene must allow one to easily determine the spatial extent and position of a dosing region, and the history of the energy deposition of the incoming electrons. The best candidates for MSX data collect events are those where the sensor measures the auroral region at different times from different directions. Measurement of the same region at two different times allows one to establish the minimum duration of the dosing and to set the time offset to be at the end of this period. This means, of course, that only the measured radiance profiles from the second measurement can be used for validation of the auroral inputs.

Table 2. SHARC parameters for IBC auroral classes.

IBC Classification	Total Electron Energy Flux (erg cm^{-2} sec^{-1})	Characteristic Energy (KeV)
II	12.9	2.9
III	100	5.0
III+	400	10.0

A number of MSX experiments satisfy these conditions. After reviewing several candidate cases with bright aurora observed in band B, one was found that satisfied all conditions and was particularly suitable due to the availability of interferometer data as well. The event, EL150400010 on 12 September in 1996, was a coordinated observation with Millstone Hill. The geomagnetic 3-hour Kp index at the time of observation was 5 and the same bright auroral arc region was observed before and after a spacecraft maneuver. Fig. 5b shows the scene created from band B measurements, where the black cone-like shape dividing the left and right portions of the image is due to a spacecraft maneuver as previously discussed. Fig. 5a depicts the viewing geometry during this event, with red lines showing the lines-of-sight (LOS) at the times of peak auroral intensity in band B measurements. Detailed examination of both figures allowed us to localize the dosed region, as indicated by the rectangular region in Fig. 5a where the lines-of-sight converge

a.
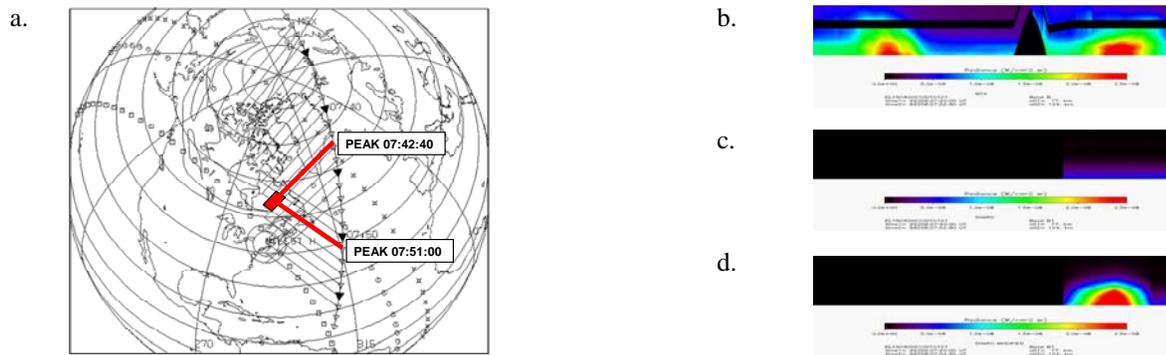
PEAK 07:42:40

PEAK 07:51:00

b.

c.

d.

Fig. 5. MSX auroral observations on September 12, 1996. a) Measurement geometry, where the red lines indicate the lines-of-sight when peak auroral emissions were observed in band B. Corner point locations for dosed region are shown where these lines-of-sight converge. b) MSX band B measurement. c) SHARC model ambient, c) SHARC model using auroral inputs determined from band B radiance profile.

As noted in our general discussion on the extraction process, it is desirable to develop additional techniques that allow us to simulate phenomena in the model environment in order to extend these capabilities to other lines-of-sight and spectral bands. We accomplished this for aurora by developing a technique to determine SHARC auroral input parameters from other measurements. We began by using MSX SPIM measurements of the 3914 Angstrom spectral emission, and we were able to validate this method using measured band B scenes of bright and weak aurora. We also developed a technique to assimilate DMSP satellite SSJ4 electron precipitation measurements in a similar

fashion. Results are shown in Fig. 6, where the DMSP F12 satellite made near-simultaneous measurements of an aurora observed in MSX band B. Fig. 6a shows orbital tracks and highlights the region of overlapping measurements in red. Fig. 6b shows the auroral scene measured by band B. Figs. 6c-e show scenes created from SHARC model runs for ambient conditions, assimilated DMSP measurements, and assimilated SPIM 3914 Angstrom measurements respectively. We contrast the ambient model scene with those created using data assimilation techniques. We also note that the assimilation based scenes compare favorably with the measured scene in terms of intensity, altitude, and spatial extent. These capabilities allow for the simulation of this auroral scene in other sensor bands for other appropriate lines-of-sight.
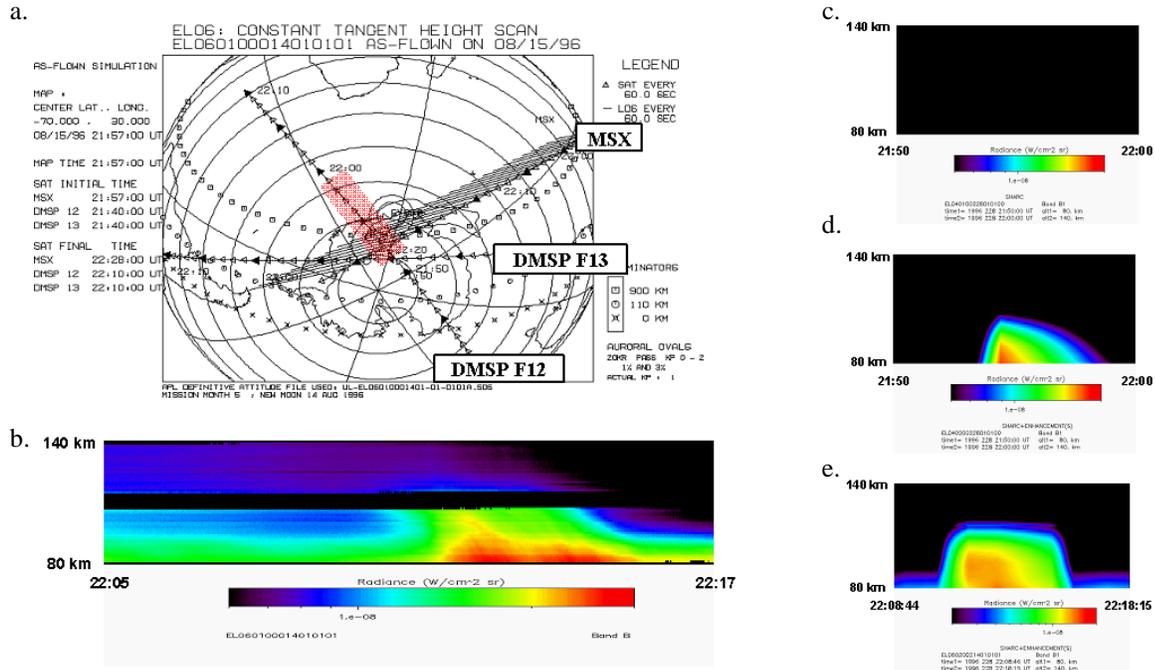
a.

c.

d.

b.

e.

Fig. 6. Aurora of 15 August 1996. a) Geographic depiction showing MSX, DMSP F12, and DMSP F13 orbital tracks. The region in red indicates near simultaneous MSX and DMSP F12 sensor coverage. b) MSX band B auroral scene measurement. SHARC model simulation using c) ambient atmosphere d) auroral inputs derived from DMSP F12 SSJ4 sensor measurements, and e) auroral inputs derived from MSX SPIM4 3914Angstrom measurements.

3.4 Nowcast and Forecast Simulations

In this section we demonstrate the utility of our empirical approach to simulating stressing radiometric conditions by creating scenarios in regions of high interest and including realistic stressing optical clutter. In the example below we describe the processes for scenario creation and band construction and demonstrate the ability to simulate scenes in other sensor bands.

As an expedient, we used MSX Earthlimb position and pointing data as the basis for constructing *pseudo-events*, where the orbital geometry and LOS conditions are replicated using the same timeline but for a different date. A series of model runs using the appropriately modified date and geophysical inputs are made to determine ambient atmospheric conditions on the new date. This allows us to account for any changes in solar flux, geomagnetic activity, and solar zenith angle. For cases where we wish to include atmospheric structure in the model, a second series of runs are made using the modified model inputs for the desired structure(s). We increased the spectral range to include 2-30 μm in order to support creation of *pseudo-sensors*, as discussed below. Tangent heights for the radiance profiles were expanded to cover an altitude range of 30-150 km. This allowed us to simulate scenes for sensors with vertical fields larger than the original MSX sensors.

For this example we illustrate an event in the vicinity of the Bering Strait. The satellite track and sensor line-of-sight are shown in Fig. 7, along with the terminator region and the region of high auroral probability. This pseudo-event shows conditions for 28 January 1997 and was constructed from an actual event on the previous day. Also shown in the figure are ambient model and simulated atmospheric structure scenes for Band B. The simulated scene includes a bright aurora over eastern Siberia and a stratospheric warming over the Bering Strait. The final product (SHARC model plus enhancement) illustrates the large impact of additional auroral radiance and the impact of stratospheric warming to the final Band B radiance.
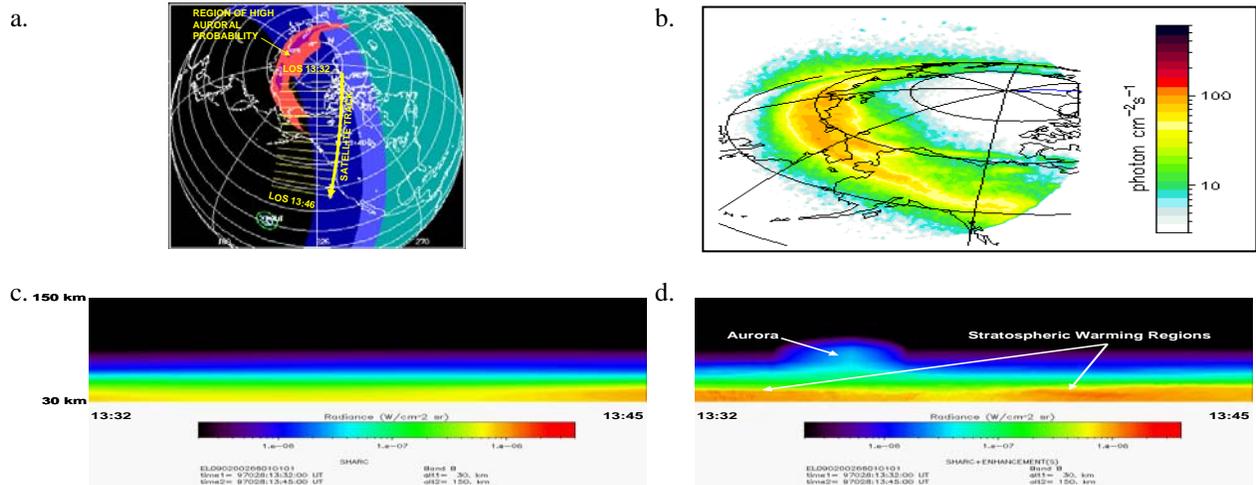

Fig. 7. Components of a simulated scene: a) the sensor satellite ground track and line-of-sight, b) LBHL auroral emission at 13:40 observed by the POLAR UVI instrument, validating our placement of a modeled aurora, c) SHARC model simulation of a Band B sensor scene from 30-150 km altitude with a benign atmospheric background, and d) SHARC model simulation with aurora and stratospheric warming added.
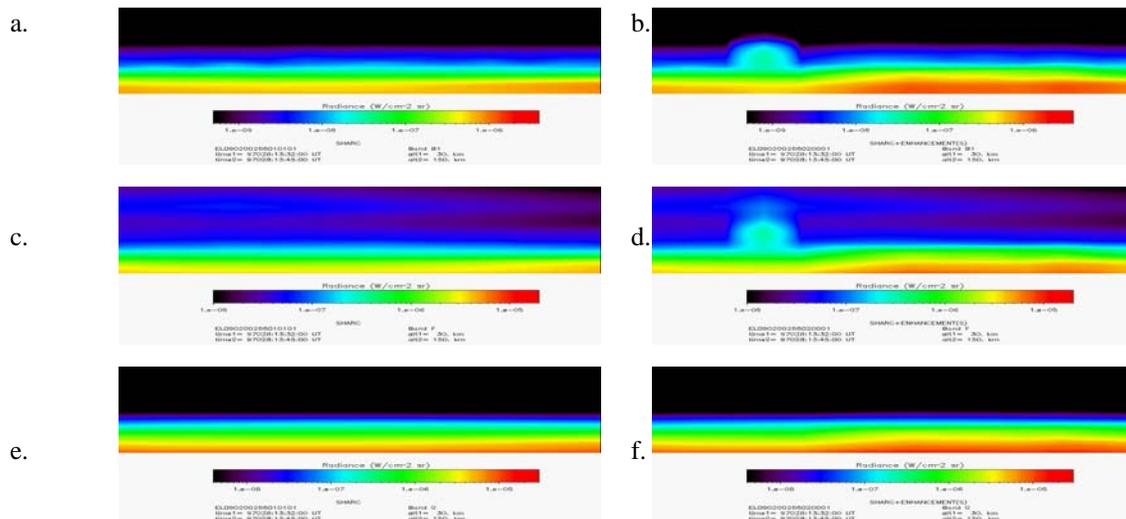

Fig. 8. Simulated sensor scenes over the Bering Strait. SHARC model simulation of a band sensor scene from 30-150km altitude: a) Band B with a benign atmospheric background, b) Band B (4.22–4.36 μm) with aurora and stratospheric warming added, c) Band F (4.00–6.00 μm) with a benign atmospheric background, d) Band F with aurora and stratospheric warming added, e) Band G (6.50–8.50 μm) with a benign atmospheric background, and f) Band G with aurora and stratospheric warming added.

The radiative transfer model provides spectral radiances for the scene. Band-integrated radiance profiles are generated in a post-processing step where the model spectral radiance is integrated over the band spectral responsivity. We constructed filter response function files for MSX Band B and two pseudo-bands, as shown in Fig. 8. In Fig. 8 we compare the simulated scenes for MSX Band B with those for the pseudo-sensor Bands F and G over the Bering Strait. The left panels of the figure show benign atmosphere scenes created from nominal SHARC model runs, while the right panels show the simulated stressing scenes for these bands. This type of analysis is useful in the sensor design process as it clearly illustrates that all of these bands are affected by the stratospheric warming, but that the choice of Band G has made it insensitive to the auroral radiance enhancement.

4. CONCLUSIONS

We have identified stressing optical clutter in atmospheric infrared measurements, determined the phenomenology responsible, and simulated this clutter in sensor scenes. Processes were developed to extract radiance enhancements from measured scenes and to add these enhancements into model-generated scenes containing benign backgrounds. We demonstrated that the extraction processes are valid by comparing individual radiance profiles produced by simulation to measured profiles. We also demonstrated that model scenes with stressing clutter added compared closely to measured scenes, and therefore these techniques are valid. A variety of phenomena were addressed, as summarized in Table 3.

Table 3. Stressing optical clutter scene simulation status.

Phenomenon	Extracted/Validated	Modeled/Validated	Climatology/Validated
Aurora	Y/Y	Y/Y	Y/Y
Temperature Inversions	Y/Y	N/N	N/N
PMC	Y/Y	N/N	Y/Y
Stratospheric Warming	Y/Y	Y/Y	N/N
Waves	Y/Y	N/N	N/N
Airglow Layer	N/N	N/N	N/N
SPRITES	N/N	N/N	N/N
Bores	N/N	N/N	N/N

We combined climatology and recent measurements with this capability to generate stressing optical clutter, and simulated sensor scenes. Our techniques addressed the spectral dependence of this clutter, so we were able to simulate sensor scenes for additional sensor bands. Because these simulated scenes were produced from validated data and processes, we consider these scenes to be valid.

5. REFERENCES

[1]   Dothe H., J.W. Duff, J.H. Gruninger, P.K. Acharya, A. Berk, and J.H. Brown, "USERS' MANUAL FOR SAMM-2, SHARC-4 and MODTRAN-4 MERGED", AFRL-VS-HA-TR-2004-1145, 2004.

[2]   Remsberg, E., G. Lingenfelser, V.L. Harvey, W. Grose, J. Russell III, M. Mlynczak, L. Gordley, and B.T. Marshall, "On the Verification of the Quality of SABER Temperature, Geopotential Height, and Wind Fields by Comparison with Met Office Assimilated Analysis", JGR 108, D20, 4628, doi:10.1029/2003JD003720,2003.

[3]   Kendra, M. J. and J. M. Griffin, "MSX: Global Radiance Database and Validation Process", AFRL-VS-TR-2001-1658, 2001.